

Supplement to:  
European NO<sub>x</sub> emissions in WRF-Chem derived from OMI:  
impacts on summertime surface ozone

Auke J. Visser<sup>1</sup>, K. Folkert Boersma<sup>1,2</sup>, Laurens N. Ganzeveld<sup>1</sup>, and Maarten C. Krol<sup>1,3</sup>

<sup>1</sup>Wageningen University, Meteorology and Air Quality Section, Wageningen, the Netherlands

<sup>2</sup>Royal Netherlands Meteorological Institute, R&D Satellite Observations, de Bilt, the Netherlands

<sup>3</sup>Institute for Marine and Atmospheric Research Utrecht, Utrecht University, Utrecht, the Netherlands

March 27, 2019

## 1 WRF-Chem namelist

Table 1: Parameterization schemes used in the WRF-Chem setup.

WRF-Chem option	Parameterization scheme (reference)
<b>Physics</b>	
Microphysics	Morrison double-moment (Morrison <i>et al.</i> , 2009)
Longwave radiation	CAM (Collins <i>et al.</i> , 2004)
Shortwave radiation	CAM (Collins <i>et al.</i> , 2004)
Surface layer	MYNN2 (Nakanishi & Niino, 2006)
Land surface physics	Noah land surface model (Tewari <i>et al.</i> , 2004)
Boundary layer physics	MYNN2 (Nakanishi & Niino, 2006; Nakanasi & Niino, 2009)
Cumulus parameterization	Grell 3D Ensemble Scheme (Grell & Devenyi, 2002)
Lightning physics	PR92 neutral buoyancy (Price & Rind, 1993)
<b>Chemistry</b>	
Gas-phase chemistry	CBM-Z (Zaveri & Peters, 1999)
Photolysis parameterization	Madronich F-TUV (Tie <i>et al.</i> , 2003)

## 2 Meteorology evaluation

### 2.1 Meteorological reanalysis data

A European-wide meteorology evaluation performed by Mar *et al.* (2016) and numerous other studies demonstrated the skill of WRF-Chem to simulate several meteorological variables relevant to O<sub>3</sub> formation (radiation, temperature, wind speed and wind direction, boundary layer height). We further evaluated WRF-Chem's performance to simulate meteorology by comparing to the ERA-Interim reanalysis product (Dee *et al.*, 2011), for five variables that are important for surface ozone: surface pressure, 2m temperature, relative humidity, wind speed and wind direction. This complements the comparison with meteorological station observations (e.g. Mar *et al.*, 2016), and has the additional advantage that it is continuous in space.

### 2.2 Results

To evaluate the meteorology in WRF-Chem we perform a comparison with the state-of-the-art ECMWF operational reanalysis product (hereafter referred to as ECMWF reanalysis). Model performance metrics for the meteorological evaluation for the two simulated months are shown in Table 2, for which show the monthly average of single-day comparisons. We only calculate performance metrics for land-based pixels, as the oceanic pixels generally contribute less to the overall bias. Overall, WRF-Chem shows good performance compared to ECMWF-reanalysis data, and WRF-Chem-ECMWF differences between March and July are consistent in sign.

WRF-Chem performs best at simulating surface temperature and pressure, but relative humidity and wind speed and -direction are simulated with less accuracy. Surface temperature is slightly underestimated, which agrees well with the cold bias generally found in WRF(-Chem) (e.g. Holtslag *et al.*, 2013; Kleczek *et al.*, 2014). Surface pressure is in general slightly underestimated, although we must note that this comparison is limited by terrain height differences in ECMWF reanalysis compared to WRF-Chem. Relative humidity is overestimated substantially in WRF-Chem, by approximately 10%. This potentially impacts simulated surface ozone in WRF-Chem, as there is an important role for surface atmospheric humidity, which governs the VPD in combination with temperature, in describing ozone removal at the surface (Kavassalis & Murphy, 2017).

We found an approximately linear increase in the model bias (defined in this section as WRF-Chem - ECMWF reanalysis) for RH in July, with a slope of 0.2% d<sup>-1</sup>. This coincides with a linear decrease in the bias from 0.12 K to -0.98 K, which would suggest that the domain-averaged latent energy flux is overestimated, leading to an enhanced moisture flux to the atmosphere and underestimated temperatures. For all other variables we did not observe a clear change in domain-average model biases with time, indicating that model performance is robust over the simulation period. Overall, this evaluation, in combination with recent WRF-Chem meteorology evaluation studies (e.g. Mar *et al.*, 2016) provides confidence in WRF-Chem's skill to reproduce domain-averaged surface meteorological conditions.

Table 2: Meteorological evaluation of two one-month WRF-Chem simulations with ECMWF operational reanalysis fields for five key surface meteorological variables. Only land-based pixels are used in the evaluation.

	March					July				
	$\mu_{ERA}$	$\mu_{WRF}$	$r^2$	MB	RMSE	$\mu_{ERA}$	$\mu_{WRF}$	$r^2$	MB	RMSE
$T_{2m}$ [K]	281.51	280.52	0.77	-0.95	2.86	296.33	295.38	0.87	-0.95	2.69
$P_{sfc}$ [hPa]	978.90	976.61	0.83	-2.29	18.56	972.94	972.28	0.96	-0.67	7.98
RH [%]	61.74	71.55	0.41	9.81	18.19	53.21	63.81	0.42	10.60	19.11
$WS_{10m}$ [m s $^{-1}$ ]	4.78	5.45	0.56	0.68	2.08	3.34	4.51	0.50	1.17	1.95
$WD_{10m}$ [°]	181.70	180.39	0.44	1.30	82.53	215.18	209.83	0.34	-5.35	85.71

### 3 Emission speciation

Table 3: Distribution of TNO-MACC non-methane VOC emission categories over VOC species in CBM-Z.

CBM-Z	TNO-MACC-III
e_ch3oh	alcohols
e_c2h5oh	alcohols
e_hc3	propane, butanes, ethyne
e_hc5	pentanes
e_hc8	hexanes & higher alkanes
e_ol2	ethene
e_olt	propene
e_oli	other alk(adi)enes & alkynes
e_tol	benzene, toluene, other aROUatics
e_xyl	xylene, trimethylbenzenes
e_hcho	methanal
e_ald	other alkanals, ethers
e_ket	ketones
e_ora2	acids

## 4 Spatial plots of emission scaling parameters

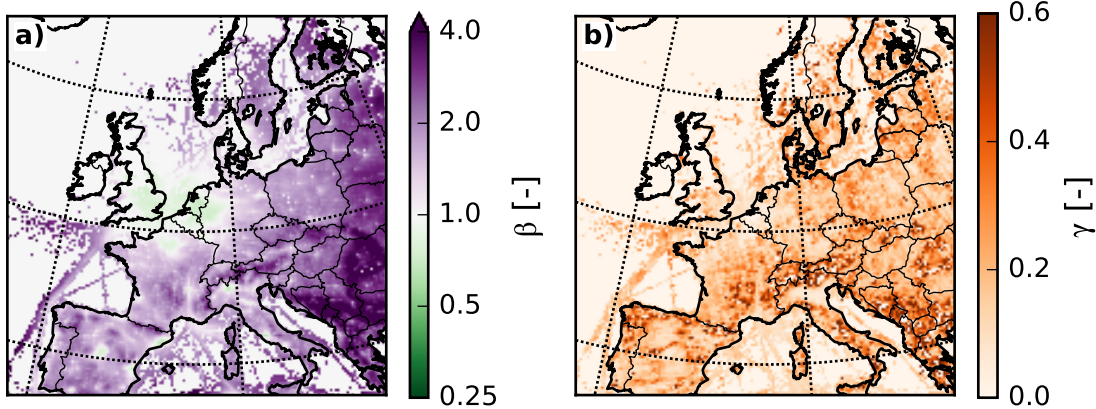


Figure 1: Spatial plots of monthly-averaged values of a)  $\beta$  and b)  $\gamma$ , calculated following Eqns. 3 and 4 (in main text), respectively.

## 5 Sensitivity study on inorganic reaction rates

A recent study investigated the representation of inorganic rate constants for tropospheric O<sub>3</sub> formation in WRF-Chem, and found a strong impact on the monthly average of 8  $\mu\text{g m}^{-3}$  when using MOZART inorganic rate constants in RADM2 (Mar et al., 2016). To evaluate the potential impact of this on our simulations, we apply the mixed-layer and chemistry model MXLCH (Janssen et al., 2012), which uses a simplified version of the MOZART mechanism. We set up this case as follows in order to reproduce polluted conditions occurring in the Mediterranean, in order to determine the impact of inorganic reaction rates on the production of ozone in a well-mixed boundary layer: The location is set at 45.5°N/3.4°E (Southern France), initial O<sub>3</sub> concentrations in the mixed layer and the free troposphere are set to 62 ppbv and 78 ppbv, respectively, initial NO and NO<sub>2</sub> concentrations in the mixed layer are set to 1.6 ppb and 4.0 ppb, respectively, we apply NO and CO emission fluxes representative for relatively polluted conditions (0.15 ppb s<sup>-1</sup> and 2.0 ppb s<sup>-1</sup>, respectively), and we add two reactions to this mechanism representing HO<sub>x</sub> cycling via reaction with O<sub>3</sub>.

From a comparison of rate constants among the mechanisms CBM-Z, RADM2 and MOZART, we found the largest differences in rate constants for the reaction forming HNO<sub>3</sub> (NO<sub>2</sub> + OH + M  $\longrightarrow$  HNO<sub>3</sub> + M), while other inorganic rate constants are much more comparable. This is in line with the rate constant comparison by Knote et al. (2015). We modify the temperature-dependent rate constants of the reaction forming HNO<sub>3</sub> ( $k_{\text{NO}_2 + \text{OH}}$ ) according to Fig. 2 (panel a), and subsequently we study the sensitivity of afternoon ozone concentrations to  $k_{\text{NO}_2 + \text{OH}}$ .

The NO<sub>2</sub> concentration and lifetime increase with decreasing rate constants, but the impact of  $k_{\text{NO}_2 + \text{OH}}$  on NO<sub>2</sub> concentrations is rather small (Fig. 2c). The relative impact on OH is stronger (Fig. 2d): the NO<sub>2</sub> availability in combination with  $k_{\text{NO}_2 + \text{OH}}$  drives OH loss, causing increasing OH concentrations for a decrease in  $k_{\text{NO}_2 + \text{OH}}$ .

HNO<sub>3</sub> formation in CBM-Z has a somewhat lower rate constant compared to other mechanisms, and therefore leads to a longer NO<sub>2</sub> lifetime. This accelerates O<sub>3</sub> formation, and thus leads to higher afternoon O<sub>3</sub> concentrations. The upper right panel of Fig. 2 shows that the inter-mechanism spread

is  $\pm 2$  ppbv. From this sensitivity analysis with a simplified representation of atmospheric chemistry within the atmospheric boundary layer, we conclude that there is some sensitivity of afternoon O<sub>3</sub> concentrations to the representation of inorganic reactions, particularly HNO<sub>3</sub> formation, involved in O<sub>3</sub> chemistry.

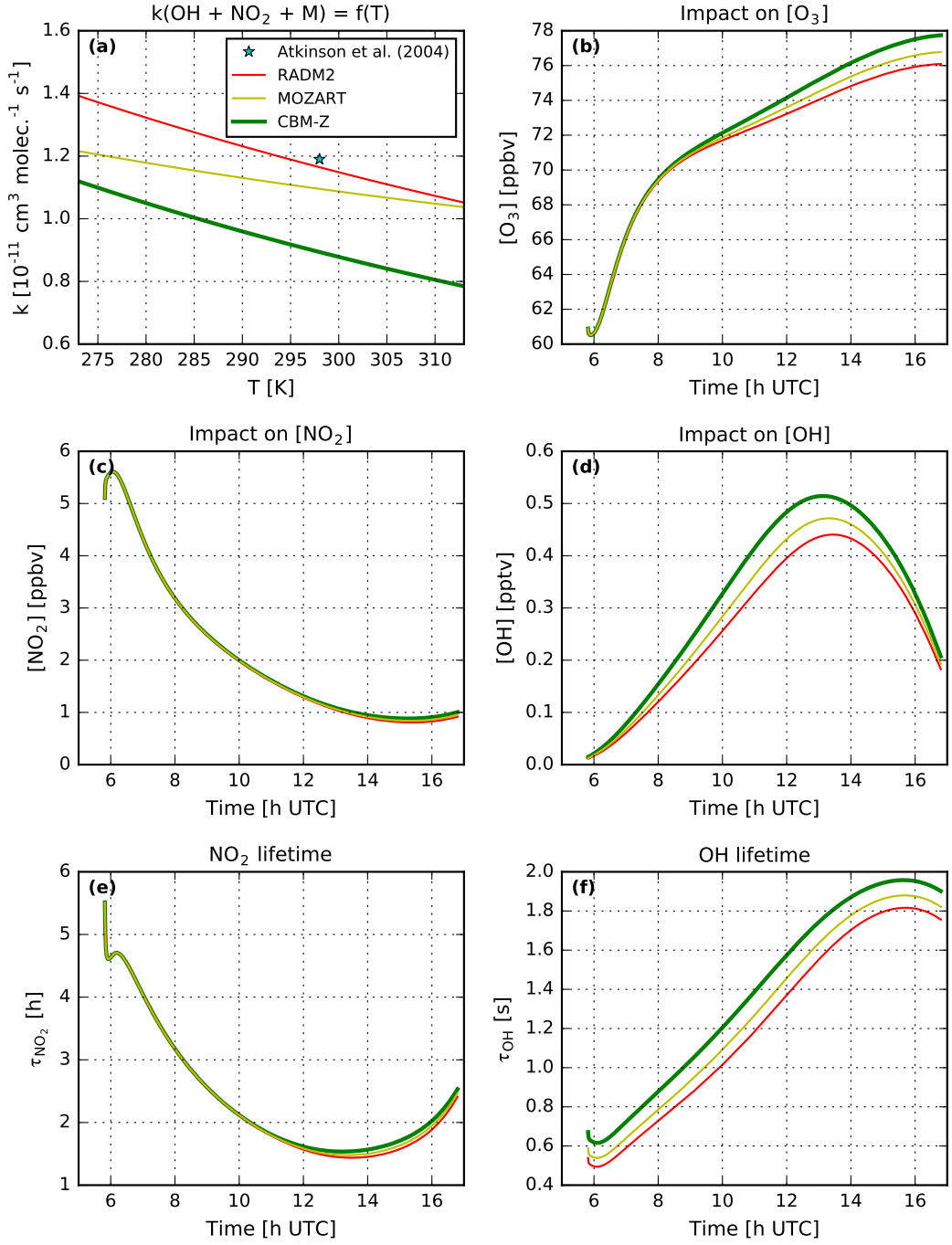


Figure 2: Temperature-dependence of rate constants for the reaction  $\text{NO}_2 + \text{OH} + \text{M} \longrightarrow \text{HNO}_3 + \text{M}$  from three different mechanisms (panel a), and the resulting impacts on  $\text{O}_3$  (pabel b),  $\text{NO}_2$  (c) and  $\text{OH}$  (d). Panel a additionally gives the IUPAC-recommended value under standard conditions ( $P = 1 \text{ bar}, T = 298 \text{ K}$ ) given by Atkinson *et al.* (2004). The lifetimes of  $\text{NO}_2$  and  $\text{OH}$  are given in panels e and f, respectively.

## References

Atkinson, R., Baulch, D. L., Cox, R. A., Crowley, J. N., Hampson, R. F., Hynes, R. G., Jenkin, M. E., Rossi, M. J., & Troe, J. 2004. Evaluated kinetic and photochemical data for atmospheric chemistry: Volume I - gas phase reactions of Ox, HOx, NOx and SOx species. *Atmospheric Chemistry and Physics*, **4**(6), 1461–1738.

Collins, W. D., Rasch, P. J., Boville, B.A., Hack, J. J., McCaa, J. R., Williamson, D. L., Kiehl, J. T., Briegleb, B., Bitz, C., Lin, S., Zhang, M., & Dai, Y. 2004. *Description of the NCAR community atmosphere model (CAM 3.0)*. Tech. rept. National Center for Atmospheric Research, Boulder, CO.

Dee, D. P., Uppala, S. M., Simmons, A. J., Berrisford, P., Poli, P., Kobayashi, S., Andrae, U., Balmaseda, M. A., Balsamo, G., Bauer, P., Bechtold, P., Beljaars, A. C M, van de Berg, L., Bidlot, J., Bormann, N., Delsol, C., Dragani, R., Fuentes, M., Geer, A. J., Haimberger, L., Healy, S. B., Hersbach, H., Hólm, E. V., Isaksen, L., Källberg, P., Köhler, M., Matricardi, M., McNally, A. P., Monge-Sanz, B. M., Morcrette, J. J., Park, B. K., Peubey, C., de Rosnay, P., Tavolato, C., Thépaut, J. N., & Vitart, F. 2011. The ERA-Interim reanalysis: Configuration and performance of the data assimilation system. *Quarterly Journal of the Royal Meteorological Society*, **137**(656), 553–597.

Grell, G. A., & Devenyi, D. 2002. A generalized approach to parameterizing convection combining ensemble and data assimilation techniques. *Geophysical Research Letters*, **29**(14), 10–13.

Holtslag, A. A.M., Svensson, G., Baas, P., Basu, S., Beare, B., Beljaars, A. C.M., Bosveld, F. C., Cuxart, J., Lindvall, J., Steeneveld, G. J., Tjernström, M., & Van De Wiel, B. J.H. 2013. Stable atmospheric boundary layers and diurnal cycles: Challenges for weather and climate models. *Bulletin of the American Meteorological Society*, **94**(11), 1691–1706.

Janssen, R. H.H., Vilà-Guerau De Arellano, J., Ganzeveld, L. N., Kabat, P., Jimenez, J. L., Farmer, D. K., Van Heerwaarden, C. C., & Mammarella, I. 2012. Combined effects of surface conditions, boundary layer dynamics and chemistry on diurnal SOA evolution. *Atmospheric Chemistry and Physics*, **12**(15), 6827–6843.

Kavassalis, Sarah C., & Murphy, Jennifer G. 2017. Understanding ozone-meteorology correlations: A role for dry deposition. *Geophysical Research Letters*, **44**(6), 2922–2931.

Kleczek, Michal A., Steeneveld, Gert Jan, & Holtslag, Albert A.M. 2014. Evaluation of the Weather Research and Forecasting Mesoscale Model for GABLS3: Impact of Boundary-Layer Schemes, Boundary Conditions and Spin-Up. *Boundary-Layer Meteorology*, **152**(2), 213–243.

Knote, C., Tuccella, P., Curci, G., Emmons, L., Orlando, J. J., Madronich, S., Baró, R., Jiménez-Guerrero, P., Luecken, D., Hogrefe, C., Forkel, R., Werhahn, J., Hirtl, M., Pérez, J. L., San José, R., Giordano, L., Brunner, D., Yahya, K., & Zhang, Y. 2015. Influence of the choice of gas-phase mechanism on predictions of key gaseous pollutants during the AQMEII phase-2 intercomparison. *Atmospheric Environment*, **115**, 553–568.

Mar, Kathleen A., Ojha, Narendra, Pozzer, Andrea, & Butler, Tim M. 2016. Ozone air quality simulations with WRF-Chem ( v3 . 5 . 1 ) over Europe : model evaluation and chemical mechanism comparison. *Geoscientific Model Development*, **9**, 3699–3728.

Morrison, H., Thompson, G., & Tatarskii, V. 2009. Impact of Cloud Microphysics on the Development of Trailing Stratiform Precipitation in a Simulated Squall Line: Comparison of One- and Two-Moment Schemes. Monthly Weather Review, **137**(3), 991–1007.

Nakanasi, M., & Niino, H. 2009. Development of an improved turbulence closure model for the atmospheric boundary layer. Journal of the Meteorological Society of Japan, **87**(5), 895–912.

Nakanishi, Mikio, & Niino, Hiroshi. 2006. An improved Mellor-Yamada Level-3 model: Its numerical stability and application to a regional prediction of advection fog. Boundary-Layer Meteorology, **119**(2), 397–407.

Price, C., & Rind, D. 1993. What determines the cloud-to-ground lightning fraction in thunderstorms? Geophysical Research Letters, **20**(6), 463–466.

Tewari, M, Chen, F, Wang, W, Dudhia, J, Lemone, M A, Mitchell, K, Ek, M, Gayno, G, Wegiel, J, & Cuenca, R H. 2004. Implementation and verification of the Unified Noah Land Surface model in the WRF model. Pages 11–15 of: 20th conference on weather analysis and forecasting/16th conference on numerical weather prediction.

Tie, Xuexi, Madronich, S., Walters, S., Zhang, R., Rasch, P. J., & Collins, William J. 2003. Effect of clouds on photolysis and oxidants in the troposphere. Journal of Geophysical Research, **108**(D20).

Zaveri, R.A., & Peters, L.K. 1999. A new lumped structure photochemical mechanism for large-scale applications. Journal of Geophysical Research: Atmospheres, **104**(D23), 30387–30415.